

Article

Effect of Relative Humidity on the Rate of New Particle Formation for Different VOCs

Austin C. Flueckiger  and Giuseppe A. Petrucci * 

Department of Chemistry, The University of Vermont, 82 University Place, Burlington, VT 05405, USA; afluecki@uvm.edu

* Correspondence: giuseppe.petrucci@uvm.edu

Abstract: Atmospheric new particle formation (NPF) is an important source of aerosol particles and cloud condensation nuclei, which affect both climate and human health. In pristine environments, oxidation of biogenic volatile organic compounds (VOCs) is a major contributor to NPF. However, the impact of relative humidity (RH) on NPF from these precursors remains poorly understood. Herein, we report on NPF, as inferred from measurements of total particle number density with a particle diameter (d_p) > 7 nm, from three VOCs (sabinene, α -terpineol, and myrtenol) subjected to dark ozonolysis. From a series of comparative experiments under humid (60% RH) and dry (~0% RH) conditions and a variety of VOC mixing ratios (ξ_{VOC} , parts per billion by volume, ppb_v), we show varied behavior in NPF at elevated RH depending on the VOC and ξ_{VOC} . In general, RH-dependent enhancement of NPF at an ξ_{VOC} between <1 ppb_v and 20 ppb_v was observed for select VOCs. Our results suggest that gaseous water *at particle genesis* enhances NPF by promoting the formation of low-volatility organic compound gas-phase products (LVOCs). This is supported by measurements of the rate of NPF for α -pinene-derived SOA, where RH had a greater influence on the initial rate of NPF than did ξ_{VOC} and ξ_{O_3} .

Keywords: secondary organic aerosol (SOA); ozonolysis; *cis*-3-hexenyl acetate (CHA); sabinene; myrtenol; α -pinene; β -pinene; α -terpineol



Citation: Flueckiger, A.C.; Petrucci, G.A. Effect of Relative Humidity on the Rate of New Particle Formation for Different VOCs. *Atmosphere* **2024**, *15*, 480. <https://doi.org/10.3390/atmos15040480>

Academic Editors: Rongzhi Tang and Wenfei Zhu

Received: 28 February 2024

Revised: 3 April 2024

Accepted: 9 April 2024

Published: 12 April 2024



Copyright: © 2024 by the authors. Licensee MDPI, Basel, Switzerland. This article is an open access article distributed under the terms and conditions of the Creative Commons Attribution (CC BY) license (<https://creativecommons.org/licenses/by/4.0/>).

1. Introduction

Understanding the chemical and physical properties of atmospheric aerosols is critical to interpreting their direct and indirect impacts on climate change, such as by scattering and absorbing solar radiation and impacting cloud formation [1–5]. Organic aerosol (OA) accounts for up to 90% of Earth’s total aerosol mass budget [6–8], with secondary organic aerosol (SOA) making up 70–90% of OA fine particle mass [9,10]. Therefore, it is of interest to study organic new particle formation (NPF) and SOA mass formation (C_{SOA}), as these processes play a crucial role in the Earth’s atmosphere.

To date, a great deal of effort has been expended to identify sources of organic particles, as well as to better understand the impact of atmospheric parameters, such as temperature, that may influence NPF. In addition to advancing our fundamental knowledge of atmospheric chemical processes, quantitative data on the role of atmospheric parameters on NPF are of interest to improve the predictive accuracy of global climate models [11,12].

Atmospheric NPF is initiated by the formation of molecular clusters, often involving atmospheric ions, sulfuric acid, water, and highly oxidized organic molecules (HOMs) [11,13–16]; moreover, it has been proposed that the incorporation of HOMs can increase cluster survivability [17–19]. Upon cluster formation, a balance exists between losses of these clusters (for example, through processes such as evaporation, condensation, and coagulation) and growth to a critical size that can facilitate atmospheric particle formation via condensation of low-volatility gas-phase products [20]. Significant effort is being expended to understand cluster formation rates and particle growth factors to more accurately quantify and predict

atmospheric NPF events [21,22] (and references therein). However, the ensuing discussion adopts a more practical view of NPF and subsequent particle growth as the emergence of new aerosol particles into the lower end of the *measured* particle size spectrum, followed by the growth of the particles [21,23].

It is generally accepted that the critical cluster size that favors survivability and growth is sub-3 nm [13,21]. Simplistically, once a critical cluster size is attained, the rate at which new particles are formed and grow to *measurable* sizes (J_{ap}) depends on the relative rates of production (P) of clusters and condensable species compared to vapor and cluster losses (L (i.e., sinks)) [23]). Hence, without fully understanding the underlying mechanisms of cluster formation and survivability, J_{ap} can be expressed as a competition between these two factors, as seen in Equation (1):

$$J_{ap} \propto P - L \quad (1)$$

By extension, any parameter that impacts either the P or the L process (or both) must, by necessity, also impact J_{ap} and NPF. For example, recent studies have shown a clear negative correlation between temperature and NPF, suggested to be due to the increased rate of production of stable clusters and lower equilibrium vapor pressures of condensable species [24–26].

Gaseous water is the third most abundant atmospheric gas; however, the mechanistic role it plays in organic NPF is not well understood. Recent reports on the effect of relative humidity (RH) on NPF have been contradictory, with a few studies reporting a positive correlation between NPF and increased humidity [27–31], while most report a negative correlation [29,32–46]. Recent work from our laboratory demonstrated both enhancement and attenuation in NPF for the dark ozonolysis of α -pinene depending on the VOC mixing ratio (ξ_{VOC} , parts per billion by volume, ppb_v) [29].

Herein, we took an empirical approach toward observing the impact of RH on SOA and NPF behavior from the ozonolysis of a variety of volatile organic compound (VOC) precursors. Specifically, we report on the effect of RH on organic NPF for three VOCs (sabinene, α -terpineol, and myrtenol) that were subjected to dark ozonolysis at various ξ_{VOCs} and ozone mixing ratios (ξ_{O_3}), and compare against previous studies that used α - and β -pinene [29] and *cis*-3-hexenyl acetate (CHA) [46]. Sabinene, α -terpineol, and myrtenol were selected for this work, as they are structural derivatives of α -pinene (RH has been shown to affect the NPF of α -pinene-derived SOA [29]), but they have varying solubilities. Of the three VOCs studied, sabinene and α -terpineol displayed enhancements in NPF under humid conditions (60% RH) relative to dry conditions (~0% RH), *specifically at* ξ_{VOCs} of less than a few ppb_v. However, myrtenol showed an attenuation in NPF under humid conditions at all ξ_{VOCs} . These results are in agreement with our recent observations from the dark ozonolysis of α - and β -pinene [29] and *cis*-3-hexenyl acetate (CHA) [46]. Our results suggest a variable correlation of NPF to increased RH at particle genesis, with a dependence on the VOC undergoing ozonolysis. In addition, the impact of ξ_{VOC} , ξ_{O_3} , and RH on the J_{ap} was examined using α -pinene as a model for VOCs that have shown NPF enhancements. NPF rate data, coupled with the observation that the highly water-soluble α -terpineol showed the greatest enhancement in NPF under humid conditions, suggests gaseous water plays a role in NPF and SOA formation through changing chemical mechanisms and/or reaction rates.

2. Materials and Methods

2.1. Reagents

The following reagents were used for this work without further purification: α -pinene (98%, CAS: 7785-70-8, Alfa Aesar, Haverhill, MA, USA), β -pinene (99%, CAS: 19902-08-0, Sigma Aldrich, St. Louis, MO, USA), sabinene (75%, CAS: 3387-41-5, Sigma Aldrich, St. Louis, MO, USA), myrtenol (97.1%, CMX: 34687, Chem-Impex International Inc., Wood Dale, IL, USA), CHA (>97.0%, CAS: 3681-71-8, TCI, Portland, OR, USA), and α -terpineol (97+%, CAS: 98-55-5, Acros Organics, Waltham, MA, USA).

2.2. Instrumentation and Experimental Conditions

Particle number concentration (N , # cm^{-3}), SOA mass (C_{SOA} , $\mu\text{g m}^{-3}$), and particle geometric mean diameter (GMD, nm) were measured or derived continuously using a scanning mobility particle sizer (SMPS 3082, TSI Inc., Shoreview, MN, USA). The SMPS utilized a long DMA and a 3756 UCPC operating at 0.3 and 3 L/min for the aerosol and sheath flow rates, respectively, resulting in a particle mobility diameter range of 17–583 nm. Rates of particle formation (J_{ap}) were determined from measurements made with an electrical low-pressure impactor (ELPI+, Dekati Technologies Ltd., Kangasala, Finland) consisting of 15 impaction stages ranging from <6 nm to 15 μm . Ozone (O_3) was produced using a commercial generator (Ozone Technologies LLC, Model 1KNT, Jersey City, NJ, USA) by passing dry, particle-free air through a corona discharge; ozone concentration was continuously monitored using a commercial unit (Serinus 10, American Ecotech, Warren, RI, USA). RH and temperature inside the chamber were monitored using a Vaisala HUMICAP[®] HMT130 dual sensor (Vaisala Inc., Vantaa, Finland). The resolution of the RH measurement was $\pm 0.1\%$. All experiments were run in batch mode and performed under ambient temperature (22 ± 1 °C) and pressure (992 ± 5 mbar) in the University of Vermont Environmental Chamber (UVMEC, Figure 1), an 8 m³ Teflon chamber equipped with multiple reagent and sampling ports. The VOC injection port was run through a magnetically coupled fan to facilitate VOC/ O_3 mixing. For all experiments (unless otherwise stated), $\xi_{\text{O}_3} = 500$ (± 30) ppb_v and the RH was either dry (~0%) or humid (60%).

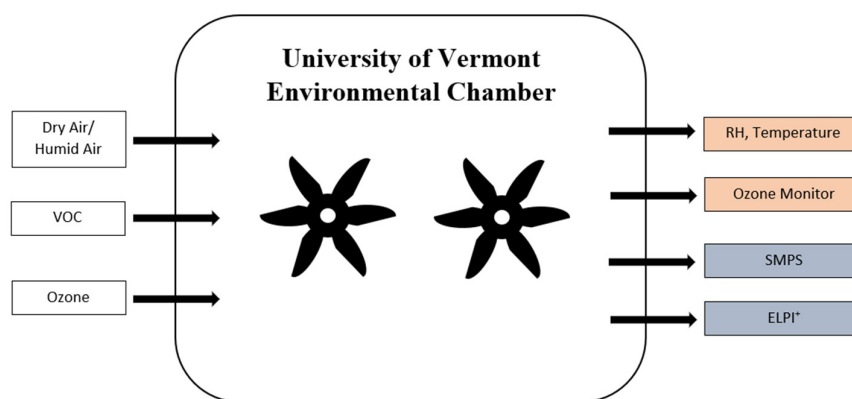


Figure 1. A schematic of the University of Vermont Environmental Chamber (UVMEC).

2.3. Data Analysis and Terminology

An **enhancement factor** (ΔN_{max} , Equation (2)) was used to quantify changes in measured NPF induced by RH:

$$\Delta N_{\text{max}} = \frac{(N_{\text{max},60\text{RH}} - N_{\text{max},0\text{RH}})}{N_{\text{max},0\text{RH}}} \quad (2)$$

here, $N_{\text{max},60\text{RH}}$ and $N_{\text{max},0\text{RH}}$ are the maximum particle number concentrations measured over the course of a humid and dry experiment, respectively. Both $N_{\text{max},60\text{RH}}$ and $N_{\text{max},0\text{RH}}$ were measured under nominally identical ξ_{VOC} and ξ_{O_3} , as ΔN_{max} is a comparative measurement. Each ΔN_{max} was determined from the average $N_{\text{max},60\text{RH}}$ and $N_{\text{max},0\text{RH}}$ of two runs at each ξ_{VOC} ; typical relative standard deviation for each metric was less than 10% [46].

The **amplification factor** (ΔE), used to describe the *sensitivity* of NPF to changes in each parameter, was determined using Equation (3):

$$\Delta E = \frac{(N_{\text{max},P} - N_{\text{max},0})}{N_{\text{max},0}} \quad (3)$$

where $N_{\text{max},P}$ is the maximum particle number concentration measured at the indicated ξ_{VOC} , ξ_{O_3} , or RH, and $N_{\text{max},0}$ is the maximum particle number concentration measured at the initial point in each respective (ξ_{VOC} , ξ_{O_3} , or RH) series. For example, if

$N_{\max} = 1.0 \times 10^3$, 6.0×10^3 , and 1.5×10^4 particles cm^{-3} for a series of three ξ_{VOCs} (e.g., $\xi_{\text{VOC}} = 10, 20$, and 30 ppb_v) run at constant ξ_{O_3} and RH (500 ppb_v and <1%, respectively), then the corresponding amplification factor for each ξ_{VOC} is $\Delta E = 0, 5$, and 14 . Therefore, it is worth noting that $\Delta E = 0$ at the initial point in each series.

2.4. Methodology

In this work, each VOC was subjected independently to dark ozonolysis under dry and humid conditions, from which ΔN_{\max} was determined using Equation (2). For a typical experiment, the UVMEC was sealed while slightly over pressure (+2 mbar) to maintain a consistent initial chamber volume. The chamber fan was then turned on and O_3 was injected for a pre-determined time pulse (typically 100–120 s) to reach $\xi_{\text{O}_3} = 500 \pm 30$ ppb_v. After an equilibration period of 10–15 min, the particle concentration was measured with the SMPS to ensure a clean background spectrum (<10 particles cm^{-3}). An optimized method of VOC injection [46] was used to improve the reproducibility of NPF and SOA generation. Briefly, the liquid aliquot of VOC was injected into a heated three-neck bulb-flask under zero-flow conditions. After 45 s, airflow was diverted through the flask to rapidly transfer a bolus of evaporated VOC to the UVMEC via a calibrated split flow valve. To reproducibly attain the low mixing ratios used in this work, the output flow from the flask passed through a split valve that allowed only a small portion (~25%) of the vaporized VOC to enter the UVMEC. The volume of liquid VOC needed to attain the desired ξ_{VOC} within the UVMEC was calculated prior to VOC injection based on the measured split ratio for each experiment. Regardless of the split ratio, the flow to the UVMEC was kept constant at 2.000 ± 0.015 L min^{-1} . Aerosol size distributions were monitored continuously for 1 h after injection of the VOC using the SMPS and ELPI+. Although we did not correct for wall losses explicitly, it was assumed that wall losses were nominally constant throughout all experiments.

3. Results and Discussion

3.1. Enhancement Factor of NPF (ΔN_{\max}) for Sabinene, α -Terpineol, and Myrtenol as a Function of ξ_{VOC}

Of the three VOCs examined, sabinene and α -terpineol displayed enhancements in NPF (i.e., positive ΔN_{\max}) under humid conditions with decreasing ξ_{VOC} ; this is in good agreement with a recent study focused on α - and β -pinene dark ozonolysis [29]. Contrary to this behavior, myrtenol exhibited an attenuation in NPF under humid conditions at all ξ_{VOCs} studied (Figure 2c), analogous to the behavior of CHA in similar experiments [46]. Figure 2 shows the N_{\max} produced for dry (tan, solid) and humid (green, hashed) experiments for the three VOCs as a function of ξ_{VOC} . Generally, as ξ_{VOC} decreased, the maximum absolute number of particles produced (regardless of RH) also decreased. However, for sabinene and α -terpineol, the particles produced under humid conditions comparatively increased relative to dry conditions as ξ_{VOC} decreased.

Table 1 summarizes the ΔN_{\max} (determined from Equation (2)) for each VOC with respect to ξ_{VOC} (shown graphically in Figure 3), along with previously reported enhancement data for α -pinene, β -pinene, and CHA. It should be noted that for cases of ξ_{VOC} where no NPF was observed (for example, α -terpineol < 1 ppb_v), it was not possible to calculate ΔN_{\max} , even if NPF was observed under humid conditions. Here, it becomes evident that the impact of RH on NPF from the ozonolysis of biogenic VOCs is variable and dependent on the molecular structure of the precursor. Although there was an attenuation in NPF and SOA formation at higher ξ_{VOCs} for all VOCs, at lower ξ_{VOCs} , only CHA and myrtenol OA continued to exhibit an attenuation in NPF and SOA mass in the presence of elevated RH at particle genesis. This latter observation is in accordance with other literature reports when working at higher ξ_{VOCs} (≥ 50 ppb_v) [29,32–46]. However, we demonstrate that even for those VOCs that suffer an attenuation in NPF and SOA mass formation under humid conditions at high ξ_{VOCs} , at lower, atmospherically relevant ξ_{VOCs} , there is an *inversion in behavior*, and an enhancement in NPF and SOA is measured in the presence of water at

particle genesis. Across all VOCs studied here, the magnitude and sign of the RH-induced effect was dependent upon the specific VOC undergoing ozonolysis.

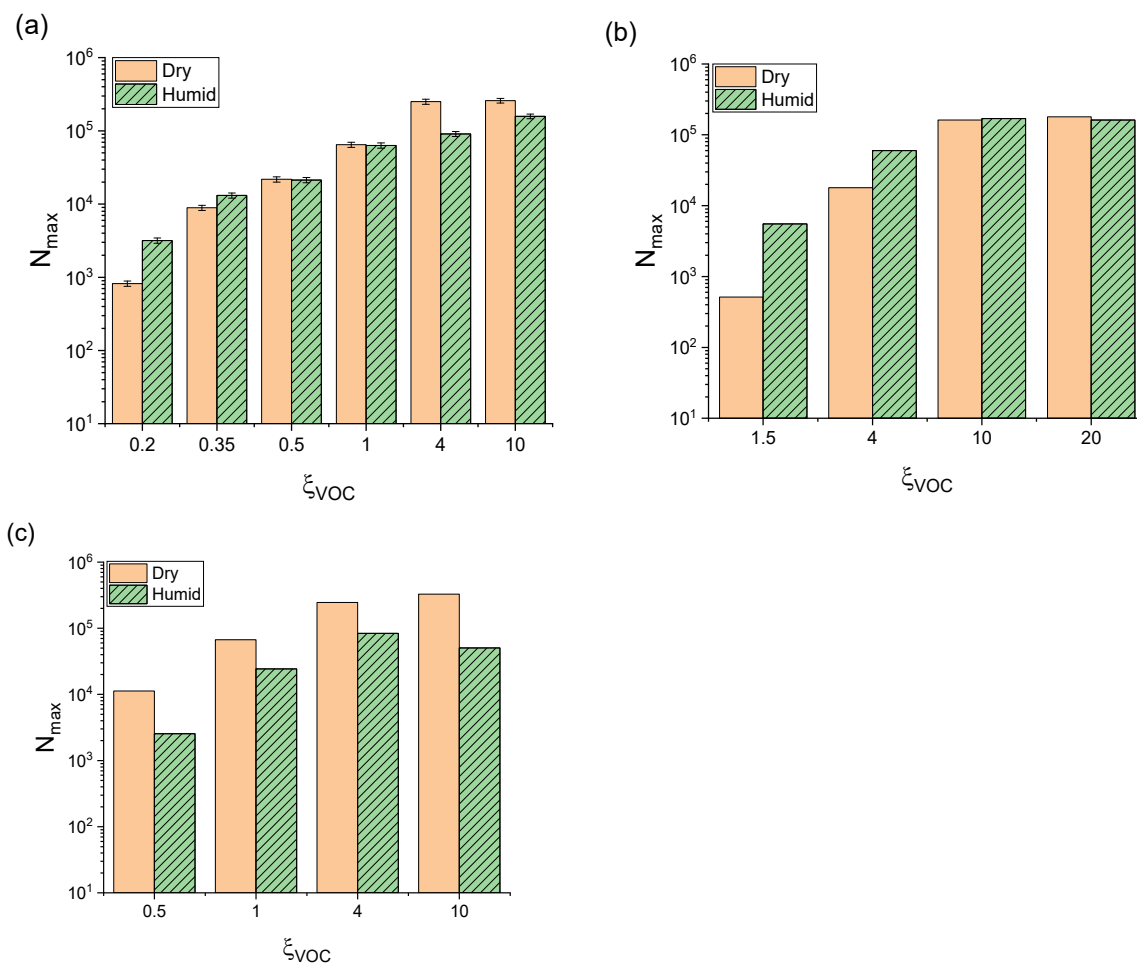


Figure 2. N_{\max} measured under dry (tan, solid) and humid (green, hashed) conditions for SOA generated by dark ozonolysis at different ξ_{VOC} s of (a) sabinene, (b) α -terpineol, and (c) myrtenol. Each bar represents the average N_{\max} ($n = 2$). Representative error bars are shown in panel (a) in accordance with previous work [47], assuming linearity in RSD with ξ_{VOC} .

Table 1. ΔN_{\max} for each VOC at varying ξ_{VOC} s. Dashes indicate that ΔN_{\max} could not be calculated at that ξ_{VOC} because no NPF was observed under dry conditions. ΔN_{\max} experiments were not conducted for sabinene and myrtenol at 20 ppb_v because it had already stabilized at lower ξ_{VOC} . Error in ξ_{VOC} estimated by propagating errors in air flow rate to chamber and syringe error. Errors in ΔN_{\max} were estimate from the RSDs interpolated for the respective $N_{\max,0\text{RH}}$ based on a previous study assessing the repeatability of SOA experiments in the UVMEC [47].

ξ_{VOC} (ppb _v)	Sabinene	α -Terpineol	Myrtenol
0.20 (± 0.02)	2.88 (± 0.25)	--	--
0.35 (± 0.03)	0.47 (± 0.04)	--	--
0.50 (± 0.03)	−0.02 (± 0.001)	--	−0.77 (± 0.06)
1.00 (± 0.03)	−0.02 (± 0.001)	--	−0.64 (± 0.02)
1.5 (± 0.03)	--	9.77 (± 0.86)	--
4.0 (± 0.1)	−0.64 (± 0.02)	2.35 (± 0.07)	−0.66 (± 0.02)
10.0 (± 0.1)	−0.39 (± 0.01)	0.04 (± 0.001)	−0.85 (± 0.03)
20.0 (± 0.3)	--	−0.09 (± 0.003)	--

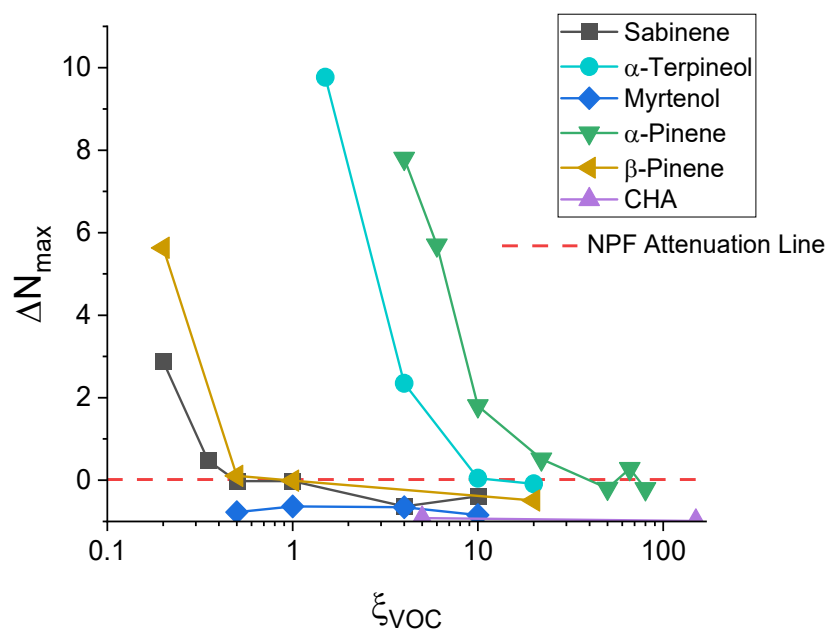


Figure 3. NPF enhancement curve for six VOCs. $\xi_{O_3} = 500$ ppb_v in all cases. RH = 60% except for β -pinene series (RH = 30%). α -Pinene, β -pinene, and CHA data incorporated from here [29,46]. For any given ξ_{VOC} , a $\Delta N_{max} < 0$ indicates an attenuation in NPF at that ξ_{VOC} , whereas a $\Delta N_{max} = -1$ indicates a complete shutdown in NPF under humid conditions at that ξ_{VOC} .

3.2. Addressing Solubility of VOCs

It is possible that the shutdown of NPF for some VOCs is due to their solubility. As discussed in a previous report [46], Teflon walls can develop a significant water film under humid conditions. This film could enhance vapor phase losses to the chamber walls of water-soluble VOCs, thereby causing a decrease in NPF. However, in accordance with the results from this previous work, the current results support the notion that the aqueous solubility of the individual VOCs does not influence the attenuation of SOA formation. As seen in Figure 4a, α -pinene, β -pinene, and sabinene, which are nearly insoluble in water (Table 2), produced an enhancement in NPF under humid conditions at low ξ_{VOCs} . CHA and myrtenol are both soluble in water (Table 2), and the ozonolysis of these VOCs at high RH resulted in an attenuation of NPF at all ξ_{VOCs} . However, α -terpineol, which is more soluble than CHA and myrtenol (by an order of magnitude), showed the greatest enhancement in NPF under humid conditions of all the VOCs studied. This would indicate that the attenuation of NPF and SOA formation is not due to loss of product to the chamber walls under humid conditions (i.e., a solubility issue) but rather that the mechanism for which gaseous water affects the formation of SOA is unique to individual VOCs.

Table 2. The VOCs addressed and their corresponding solubility. * Solubilities as reported in <https://pubchem.ncbi.nlm.nih.gov/> (accessed on 23 February 2024).

VOC	Solubility in H ₂ O (mg/L) *
Sabinene	2.5
α -Terpineol	7100
Myrtenol	427
α -Pinene	Insoluble
β -Pinene	Insoluble
CHA	900

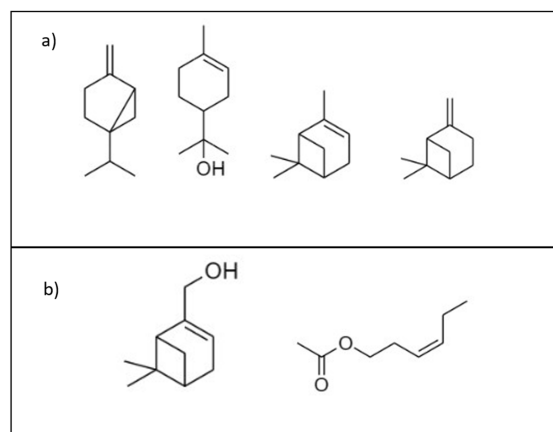


Figure 4. (a) The four VOCs that resulted in an enhancement of NPF under humid conditions: sabinene, α -terpineol, α -pinene, and β -pinene (from left to right). (b) The two VOCs that resulted in a shutdown of NPF under humid conditions at all ξ_{VOCs} : myrtenol and CHA (left to right).

3.3. Effect of RH on the Rate of NPF for α -Pinene-Derived SOA

3.3.1. Effect of ξ_{VOC} , ξ_{O_3} , and RH on ΔN_{max}

Three of the controllable variables that affect the formation of SOA at particle genesis in our batch-mode atmospheric chamber experiments were ξ_{VOC} , ξ_{O_3} , and RH. It was determined that all three variables had an influence on ΔN_{max} (Figure 5). Under constant ξ_{O_3} (500 ppb_v), there existed a non-linear increase in ΔN_{max} as ξ_{VOC} decreased (Figure 5a). By increasing ξ_{O_3} while keeping a fixed ξ_{VOC} (10 ppb_v), ΔN_{max} generally increased (Figure 5b), as one would expect. Similarly, Figure 5c shows an increase in ΔN_{max} with increasing “humid” RH (ξ_{VOC} and ξ_{O_3} fixed at 10 and 500 ppb_v, respectively) compared to ~0% RH. Although the greatest enhancement of ΔN_{max} was influenced by a decrease in ξ_{VOC} , it is evident that all three chamber variables had an influence on ΔN_{max} at low ξ_{VOCs} . It is important to note that the relative importance of each parameter may depend on the absolute value of the parameter that remains fixed. For example, the ΔN_{max} corresponding to ξ_{VOC} may have differed if the fixed $\xi_{\text{O}_3} = 10$ ppb_v rather than 500 ppb_v. For the present study, each fixed parameter was chosen to permit comparison with other work in our laboratory [29,46,47] and in the literature.

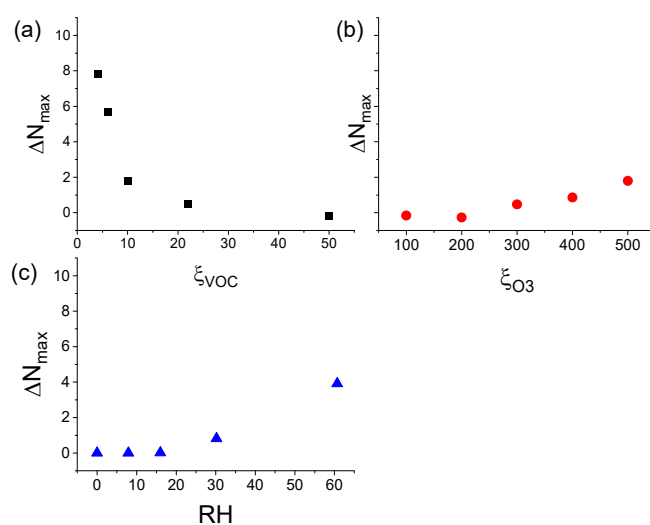


Figure 5. Enhancement factor of α -pinene-derived SOA corresponding to varying one of three particle genesis conditions: (a) ξ_{VOC} (black, $\xi_{\text{O}_3} = 500$ ppb_v), (b) ξ_{O_3} (red, $\xi_{\text{VOC}} = 10$ ppb_v), and (c) RH (blue, $\xi_{\text{O}_3} = 500$ ppb_v and $\xi_{\text{VOC}} = 10$ ppb_v). All are scaled to a ΔN_{max} of 11 to show the relative impact of each condition on the enhancement of NPF.

3.3.2. Effect of ξ_{VOC} , ξ_{O_3} , and RH on ΔE

The sensitivity of NPF from the dark ozonolysis of α -pinene to each chamber variable was quantified by way of the amplification factor (ΔE , comparative measure of the maximum particle number concentration produced at the given $\xi_{\text{VOC}}/\xi_{\text{O}_3}/\text{RH}$ relative to the initial point in each respective series). ΔE was derived from Equation (3) and assessed for each chamber variable (Figure 6). The y-axis is scaled to provide a direct, visual comparison of the enhancement between the three variables. Figure 6a shows that an increase in ξ_{VOC} with static ξ_{O_3} and RH (500 ppb_v and ~0%) led to an increase in ΔE . Similarly, Figure 6c shows that an increase in RH with static ξ_{VOC} and ξ_{O_3} (10 ppb_v and 500 ppb_v) also yielded a general increase in ΔE . However, somewhat surprisingly, this is not the case for an increase in ξ_{O_3} (Figure 6b), which yielded little to no change in ΔE (static ξ_{VOC} of 10 ppb_v and RH of ~0%), suggesting that regardless of the absolute value of ξ_{O_3} , the system's sensitivity to changes in the parameter remains constant.

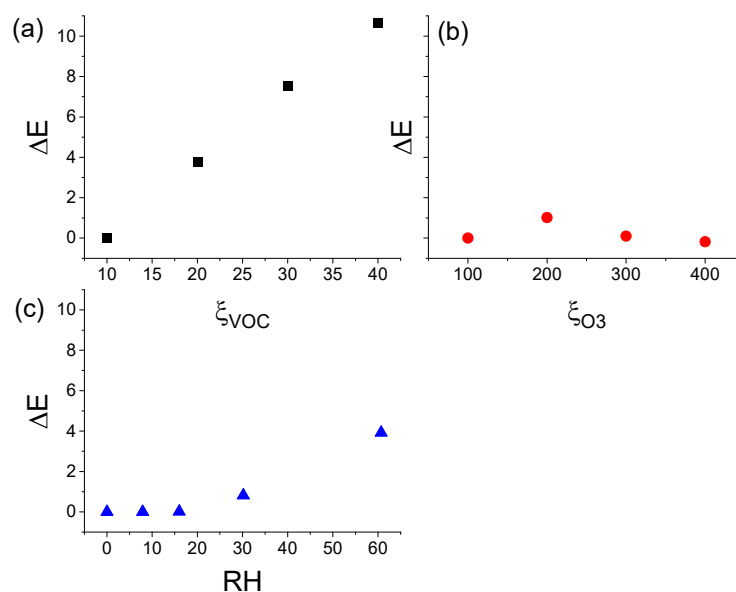


Figure 6. Amplification factor of α -pinene-derived SOA for three chamber parameters: (a) ξ_{VOC} (black), (b) ξ_{O_3} (red), and (c) RH (blue). All plots are scaled to a maximum ΔE of 11 to show the relative impact of each condition on the enhancement of NPF.

3.3.3. Effect of ξ_{VOC} , ξ_{O_3} , and RH on J_{ap}

To shed light on the effect of RH on NPF for the VOCs that exhibited an enhancement under humid conditions, a systematic study was conducted by which the effect of varying chamber conditions on the apparent rate of particle formation (J_{ap}) was examined. For this work, α -pinene-derived SOA was used as an example for the VOCs that exhibited an enhancement in NPF.

The general trends in normalized J_{ap} (Figure 7) match comparatively with the general trends for ΔE in each series (Figure 6), where increases in ξ_{VOC} and RH enhanced the apparent rate of particle formation but ξ_{O_3} did not. Although the absolute increase in J_{ap} with respect to ξ_{VOC} was greater than that with respect to RH (Figure 7a compared to Figure 7c), when plotting J_{ap} vs. ΔE (Figure 8), the slope of the log–log plot for RH-dependent J_{ap} was approximately 16 times greater than the ξ_{VOC} -dependent J_{ap} . This indicates that at low ξ_{VOC} of α -pinene, at particle genesis, *changes in RH have a much greater impact on the apparent rate at which the OA particles form compared to the ξ_{VOC} and ξ_{O_3}* . This would indicate that RH-dependent rates of NPF are likely a major driving force of the eight-fold enhancement in NPF for α -pinene-derived SOA (seen here: Snyder et al. [29]).

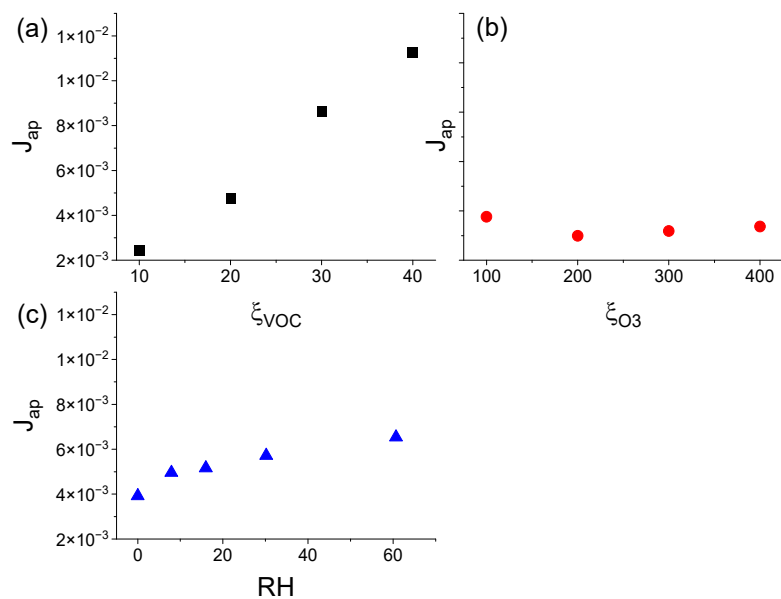


Figure 7. The normalized apparent rate of particle formation (J_{ap}) of α -pinene-derived SOA, corresponding to three particle genesis conditions: (a) ξ_{VOC} (black), (b) ξ_{O3} (red), and (c) RH (blue). All are scaled to a ΔE of 11 to show the relative impact of each condition on the enhancement of NPF.

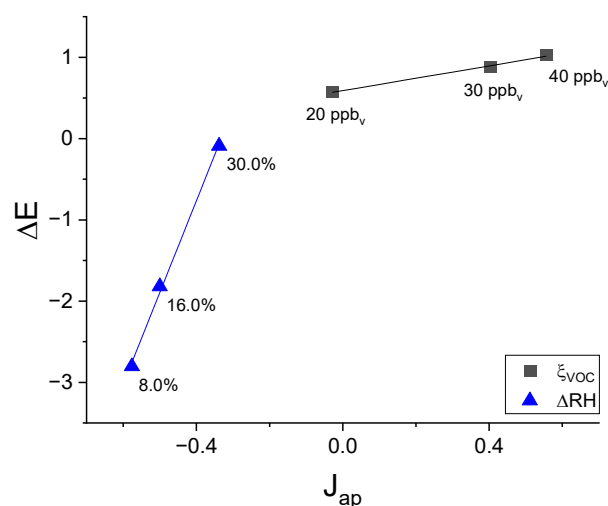


Figure 8. Log–log plot of amplification factor (ΔE) vs. normalized apparent rate of particle formation (J_{ap}) for ξ_{VOC} (black squares) and RH (blue triangles) of α -pinene-derived SOA. The slope of the RH series is approximately $16\times$ greater than that of the ξ_{VOC} series.

In a study conducted by Chu et al. [48], the authors discuss the increased deviation in experimental aerosol formation from their predicted models corresponding to increased RH. The possible explanation posed is that the gaseous water would be taken up by particles, leading to greater surface area and subsequently growing the condensation sink for gas-phase products to partition onto. Although plausible at higher ξ_{VOCs} , where we also see an attenuation in NPF with elevated RH for all VOCs, *that explanation does not fit our observations at low ξ_{VOCs}* . At low ξ_{VOCs} , for certain VOCs, it appears as though the presence of gaseous water (in excess compared to the concentration of the VOC) led to a promotion of OH reactivity prior to ozonolysis of the VOC [49,50], which seemingly promotes low-volatility organic compound (LVOC) gas-phase product formation and subsequent nucleating species that yield NPF events at a greater rate than when ξ_{VOCs} are higher. This is supported by the observation (Figure 8) that ΔE showed a $16\times$ greater dependence on RH than ξ_{VOC} .

Regarding pristine environments, pure organic NPF has also been observed [51–56], and the theoretical underpinning of organic cluster formation and nucleation has recently been reviewed [19]. Here, it is proposed that pure organic clusters are formed and perhaps stabilized by water molecules or dimers in direct relation to the vapor pressure of the oxidized products and their gas-phase concentrations. If the instantaneous gas-phase concentration of an oxidation product is greater than its equilibrium vapor pressure (i.e., the system is supersaturated in that product), then the probability of cluster formation and NPF increases (see, for example, [48,55,57–59]). This supposition is supported by recent laboratory studies that showed that decreases in system temperature (i.e., decreases in equilibrium vapor pressure) resulted in significant enhancements in NPF [24–26]. This enhancement was observed despite decreases in the formation of HOMs at lower temperatures [60].

Elevated RH is likely to increase L (Equation (1)) through processes such as enhanced coagulation scavenging of newly formed clusters and condensable gases [61], as well as increased coagulation and scavenging rates of ultrafine particles [42,62]. For example, water vapor uptake to particles could reduce organic (equilibrium) partial pressures according to Raoult's law. Particle deliquescence would significantly dilute the organics in the particles, resulting in a reduction in organic partial pressures according to Raoult's law [63–66]. In addition, an aqueous phase could attract water-soluble organics according to Henry's law. Lastly, humidity on chamber walls may have an outsized impact on losses of ultrafine particles, which generally suffer greater wall loss rates than larger particles [67]. Therefore, as wall losses could increase at higher RH, the results reported herein could be interpreted as lower limits of the enhancements in NPF as a function of RH.

By all accounts, increases in particle liquid water (PLW) enhance the partitioning of semi- and low-volatility gas-phase products (S- and LVOCs) to the organic particulate (due to a lowering of the average molecular weight of particle constituents) [68–72]. Furthermore, PLW has been shown to increase particle diffusivity, enhancing condensation rates to organic particles [65,71,73–75]. Again, both of these effects would result in an increased sink (i.e., L , Equation (1)) at higher RH. The main L for newly formed particles in the atmosphere is coagulation onto an existing particle population [76], whereas in chamber experiments, the main L stems from particle losses to chamber walls, which are normally much more important than coagulation [77] because the existing particle population is usually absent or small. It cannot be discounted that elevated RH could lead to decreased vapor-phase wall losses, thereby increasing the concentration of LVOCs in the gas phase (C_{LVOC} considered analogous to the yield of LVOCs, ϕ_{LVOC} , used by Chu et al. [71]), which could favor NPF. There is only one case, however, of which the authors are aware where increased relative humidity resulted in very modest mitigation of gas-phase wall losses [61]. This singular case studied the loss of oxygenated vapors resulting from the reaction of OH with toluene, a very different chemical system from the current study.

Therefore, RH is likely playing a role by increasing P (Equation (1)) by any number of processes, such as modified oxidized product distributions, enhanced formation of nucleating species, enhanced rate of cluster formation, and/or enhanced survivability (i.e., stabilization) of clusters [31]. Regardless of the precise mechanism(s) by which NPF is impacted by the presence of water, therefore, it appears likely that an increase in water concentration must, by a gas-phase reaction, produce more LVOCs or the rates of production of LVOCs must be greater, effectively outcompeting vapor sinks such as condensation and partitioning in the presence of seed particles or, perhaps, coagulation and wall loss effects (both gas and particle) common in chamber experiments (see Charan et al. [78] for an excellent review on the topic).

4. Conclusions

Overall, the correlation between RH and organic NPF is variable, with a significant dependence on the specific VOC undergoing ozonolysis. In this work, three VOCs (sabinene, α -terpineol, and myrtenol) were subjected to dark ozonolysis under dry and humid conditions (~0 and 60% RH, respectively) at a variety of ξ_{VOCs} . When incorporating data

from our previous work [29,46], four VOCs (α -pinene, β -pinene, sabinene, and α -terpineol) displayed enhancements in NPF under humid conditions as the ξ_{VOC} decreased; however, myrtenol and CHA showed an attenuation in NPF under humid conditions for all ξ_{VOCs} . For the VOCs that had NPF enhancements, gaseous water likely played a crucial role in the chemical formation of low-volatility gas-phase products at low ξ_{VOCs} . Therefore, these low-volatility products would have spawned new and more frequent NPF events compared to those at high ξ_{VOCs} and/or dry conditions. In addition, we note that the observed behavior is not solely due to a VOC's solubility; this is supported by our observation where α -terpineol produced the greatest ΔN_{max} despite its solubility being an order of magnitude greater than that of CHA and myrtenol.

Furthermore, as a proof-of-concept study, α -pinene was used as a model to systematically probe the effect of each chamber variable (ξ_{VOC} , ξ_{O_3} , and RH) on the observed enhancement in NPF. Here, it was determined that the ΔN_{max} and ΔE were dependent on all three chamber variables (ξ_{VOC} , ξ_{O_3} , and RH), while J_{ap} was independent of ξ_{O_3} . However, of the two dependences (ξ_{VOC} and RH), when compared to their respective amplification factors, the sensitivity of NPF was influenced more by RH than by ξ_{VOC} (approximately $16\times$). Therefore, for the VOCs that exhibit NPF enhancements at low ξ_{VOCs} , the presence of gaseous water at particle genesis during ozonolysis is shown to be the driving force behind the production of enhanced NPF events.

The role of humidity in atmospheric organic NPF is complex and dependent on the specific SOA precursor under consideration. Furthermore, while the current study focused primarily on two RH levels ($\sim 0\%$ reflective of most laboratory studies of SOA and 60% reflective of the average global RH), the preliminary results from α -pinene clearly point to the need to study systematically these effects at intermediate RHs reflective of different environments. It may be possible that upon more extensive experimentation with a broader range of VOCs and across a secondary dimension of RH for each VOC, general parameters may be derived to facilitate incorporation of these effects into climate models to improve outcomes.

Author Contributions: A.C.F. and G.A.P. contributed equally to the ideation of the experiments. A.C.F. carried out all experiments. G.A.P. supervised all laboratory activities. All authors contributed to the preparation of this manuscript. All authors have read and agreed to the published version of the manuscript.

Funding: This material is based upon work supported by the National Science Foundation under Grant No. CHE-1709751.

Institutional Review Board Statement: Not applicable.

Informed Consent Statement: Not applicable.

Data Availability Statement: The data presented in this study are available on request from the corresponding author.

Conflicts of Interest: The authors declare no conflicts of interest.

References

1. Forster, P.; Storelvmo, T.; Armour, K.; Collins, W.; Dufresne, J.-L.; Frame, D.; Lunt, D.J.; Mauritsen, T.; Palmer, M.D.; Watanabe, M.; et al. *Climate Change 2021—The Physical Science Basis: Working Group I, the Earth's Energy Budget, Climate Feedbacks and Climate Sensitivity*; IPCC: Geneva, Switzerland, 2023; pp. 923–1054.
2. Zhang, C.Q.; Guo, Y.D.; Shen, H.R.; Luo, H.; Pullinen, I.; Schmitt, S.H.; Wang, M.J.; Fuchs, H.; Kiendler-Scharr, A.; Wahner, A.; et al. Contrasting Influence of Nitrogen Oxides on the Cloud Condensation Nuclei Activity of Monoterpene-Derived Secondary Organic Aerosol in Daytime and Nighttime Oxidation. *Geophys. Res. Lett.* **2023**, *50*, e2022GL102110. [[CrossRef](#)]
3. Jo, D.S.; Nault, B.A.; Tilmes, S.; Gettelman, A.; Mccluskey, C.S.; Hodzic, A.; Henze, D.K.; Nawaz, M.O.; Fung, K.M.; Jimenez, J.L. Global Health and Climate Effects of Organic Aerosols from Different Sources. *Environ. Sci. Technol.* **2023**, *57*, 13793–13807. [[CrossRef](#)] [[PubMed](#)]
4. Li, J.; Carlson, B.E.; Yung, Y.L.; Lv, D.R.; Hansen, J.; Penner, J.E.; Liao, H.; Ramaswamy, V.; Kahn, R.A.; Zhang, P.; et al. Scattering and absorbing aerosols in the climate system. *Nat. Rev. Earth Environ.* **2022**, *3*, 363–379. [[CrossRef](#)]

5. Shrivastava, M.; Cappa, C.D.; Fan, J.; Goldstein, A.H.; Guenther, A.B.; Jimenez, J.L.; Kuang, C.; Laskin, A.; Martin, S.T.; Ng, N.L.; et al. Recent advances in understanding secondary organic aerosol: Implications for global climate forcing. *Rev. Geophys.* **2017**, *55*, 509–559. [[CrossRef](#)]
6. Ehn, M.; Thornton, J.A.; Kleist, E.; Sipila, M.; Junninen, H.; Pullinen, I.; Springer, M.; Rubach, F.; Tillmann, R.; Lee, B.; et al. A large source of low-volatility secondary organic aerosol. *Nature* **2014**, *506*, 476–479. [[CrossRef](#)] [[PubMed](#)]
7. Hallquist, M.; Wenger, J.C.; Baltensperger, U.; Rudich, Y.; Simpson, D.; Claeys, M.; Dommen, J.; Donahue, N.M.; George, C.; Goldstein, A.H.; et al. The formation, properties and impact of secondary organic aerosol: Current and emerging issues. *Atmos. Chem. Phys.* **2009**, *9*, 5155–5236. [[CrossRef](#)]
8. Jimenez, J.L.; Canagaratna, M.R.; Donahue, N.M.; Prevot, A.S.H.; Zhang, Q.; Kroll, J.H.; DeCarlo, P.F.; Allan, J.D.; Coe, H.; Ng, N.L.; et al. Evolution of Organic Aerosols in the Atmosphere. *Science* **2009**, *326*, 1525–1529. [[CrossRef](#)]
9. Kanakidou, M.; Seinfeld, J.H.; Pandis, S.N.; Barnes, I.; Dentener, F.J.; Facchini, M.C.; Van Dingenen, R.; Ervens, B.; Nenes, A.; Nielsen, C.J.; et al. Organic aerosol and global climate modelling: A review. *Atmos. Chem. Phys.* **2005**, *5*, 1053–1123. [[CrossRef](#)]
10. Shrivastava, M.; Easter, R.C.; Liu, X.H.; Zelenyuk, A.; Singh, B.; Zhang, K.; Ma, P.L.; Chand, D.; Ghan, S.; Jimenez, J.L.; et al. Global transformation and fate of SOA: Implications of low-volatility SOA and gas-phase fragmentation reactions. *J. Geophys. Res. Atmos.* **2015**, *120*, 4169–4195. [[CrossRef](#)]
11. Olenius, T.; Bergström, R.; Kubecka, J.; Myllys, N.; Elm, J. Reducing chemical complexity in representation of new-particle formation: Evaluation of simplification approaches. *Environ. Sci. Atmos.* **2023**, *3*, 552–567. [[CrossRef](#)]
12. Bender, F.A.M.; Frey, L.; McCoy, D.T.; Grosvenor, D.P.; Mohrmann, J.K. Assessment of aerosol-cloud-radiation correlations in satellite observations, climate models and reanalysis. *Clim. Dyn.* **2019**, *52*, 4371–4392. [[CrossRef](#)]
13. Kulmala, M.; Petaja, T.; Ehn, M.; Thornton, J.; Sipila, M.; Worsnop, D.R.; Kerminen, V.M. Chemistry of Atmospheric Nucleation: On the Recent Advances on Precursor Characterization and Atmospheric Cluster Composition in Connection with Atmospheric New Particle Formation. *Annu. Rev. Phys. Chem.* **2014**, *65*, 21–37. [[CrossRef](#)] [[PubMed](#)]
14. Stolzenburg, D.; Cai, R.L.; Blichner, S.M.; Kontkanen, J.; Zhou, P.T.; Makkonen, R.; Kerminen, V.M.; Kulmala, M.; Riipinen, I.; Kangasluoma, J. Atmospheric nanoparticle growth. *Rev. Mod. Phys.* **2023**, *95*, 045002. [[CrossRef](#)]
15. Kirkby, J.; Amorim, A.; Baltensperger, U.; Carslaw, K.S.; Christoudias, T.; Curtius, J.; Donahue, N.M.; El Haddad, I.; Flagan, R.C.; Gordon, H.; et al. Atmospheric new particle formation from the CERN CLOUD experiment. *Nat. Geosci.* **2023**, *16*, 948–957. [[CrossRef](#)]
16. Zhang, R.Y.; Khalizov, A.; Wang, L.; Hu, M.; Xu, W. Nucleation and Growth of Nanoparticles in the Atmosphere. *Chem. Rev.* **2012**, *112*, 1957–2011. [[CrossRef](#)]
17. Riccobono, F.; Schobesberger, S.; Scott, C.E.; Dommen, J.; Ortega, I.K.; Rondo, L.; Almeida, J.; Amorim, A.; Bianchi, F.; Breitenlechner, M.; et al. Oxidation Products of Biogenic Emissions Contribute to Nucleation of Atmospheric Particles. *Science* **2014**, *344*, 717–721. [[CrossRef](#)] [[PubMed](#)]
18. Kupc, A.; Williamson, C.J.; Hodshire, A.L.; Kazil, J.; Ray, E.; Bui, T.P.; Dollner, M.; Froyd, K.D.; McKain, K.; Rollins, A.; et al. The potential role of organics in new particle formation and initial growth in the remote tropical upper troposphere. *Atmos. Chem. Phys.* **2020**, *20*, 15037–15060. [[CrossRef](#)]
19. Elm, J.; Ayoubi, D.; Engsvang, M.; Jensen, A.B.; Knattrup, Y.; Kubecka, J.; Bready, C.J.; Fowler, V.R.; Harold, S.E.; Longworth, O.M.; et al. Quantum chemical modeling of organic enhanced atmospheric nucleation: A critical review. *Wires Comput. Mol. Sci.* **2023**, *13*, 1662. [[CrossRef](#)]
20. Li, C.X.; Zhao, Y.; Li, Z.Y.; Liu, L.; Zhang, X.H.; Zheng, J.; Kerminen, V.M.; Kulmala, M.; Jiang, J.K.; Cai, R.L.; et al. The dependence of new particle formation rates on the interaction between cluster growth, evaporation, and condensation sink. *Environ. Sci. Atmos.* **2023**, *3*, 168–181. [[CrossRef](#)]
21. Dada, L.; Lehtipalo, K.; Kontkanen, J.; Nieminen, T.; Baalbaki, R.; Ahonen, L.; Duplissy, J.; Yan, C.; Chu, B.W.; Petaja, T.; et al. Formation and growth of sub-3-nm aerosol particles in experimental chambers. *Nat. Protoc.* **2020**, *15*, 1013–1040. [[CrossRef](#)]
22. Li, C.X.; Signorell, R. Understanding vapor nucleation on the molecular level: A review. *J. Aerosol Sci.* **2021**, *153*, 105676. [[CrossRef](#)]
23. Kerminen, V.M.; Chen, X.M.; Vakkari, V.; Petaja, T.; Kulmala, M.; Bianchi, F. Atmospheric new particle formation and growth: Review of field observations. *Environ. Res. Lett.* **2018**, *13*, 103003. [[CrossRef](#)]
24. Deng, Y.G.; Inomata, S.; Sato, K.; Ramasamy, S.; Morino, Y.; Enami, S.; Tanimoto, H. Temperature and acidity dependence of secondary organic aerosol formation from alpha-pinene ozonolysis with a compact chamber system. *Atmos. Chem. Phys.* **2021**, *21*, 5983–6003. [[CrossRef](#)]
25. Heinritzi, M.; Dada, L.; Simon, M.; Stolzenburg, D.; Wagner, A.C.; Fischer, L.; Ahonen, L.R.; Amanatidis, S.; Baalbaki, R.; Baccarini, A.; et al. Molecular understanding of the suppression of new-particle formation by isoprene. *Atmos. Chem. Phys.* **2020**, *20*, 11809–11821. [[CrossRef](#)]
26. Kristensen, K.; Jensen, L.N.; Quelever, L.L.J.; Christiansen, S.; Rosati, B.; Elm, J.; Teiwes, R.; Pedersen, H.B.; Glasius, M.; Ehn, M.; et al. The Aarhus Chamber Campaign on Highly Oxygenated Organic Molecules and Aerosols (ACCHA): Particle formation, organic acids, and dimer esters from alpha-pinene ozonolysis at different temperatures. *Atmos. Chem. Phys.* **2020**, *20*, 12549–12567. [[CrossRef](#)]
27. Jonsson, A.M.; Hallquist, M.; Ljungstrom, E. Impact of humidity on the ozone initiated oxidation of limonene, Delta(3)-carene, and alpha-pinene. *Environ. Sci. Technol.* **2006**, *40*, 188–194. [[CrossRef](#)] [[PubMed](#)]

28. Yu, K.P.; Lin, C.C.; Yang, S.C.; Zhao, P. Enhancement effect of relative humidity on the formation and regional respiratory deposition of secondary organic aerosol. *J. Hazard. Mater.* **2011**, *191*, 94–102. [[CrossRef](#)] [[PubMed](#)]
29. Snyder, C.N.; Flueckiger, A.C.; Petrucci, G.A. Relative Humidity Impact on Organic New Particle Formation from Ozonolysis of α - and β -Pinene at Atmospherically Relevant Mixing Ratios. *Atmosphere* **2023**, *14*, 173. [[CrossRef](#)]
30. Huang, Y.; Ho, K.F.; Ho, S.S.H.; Lee, S.C.; Yau, P.S.; Cheng, Y. Physical parameters effect on ozone-initiated formation of indoor secondary organic aerosols with emissions from cleaning products. *J. Hazard. Mater.* **2011**, *192*, 1787–1794. [[CrossRef](#)]
31. Jonsson, Å.M.; Hallquist, M.; Ljungström, E. The effect of temperature and water on secondary organic aerosol formation from ozonolysis of limonene, Δ^3 -carene and α -pinene. *Atmos. Chem. Phys.* **2008**, *8*, 6541–6549. [[CrossRef](#)]
32. Bousiotis, D.; Brean, J.; Pope, F.D.; Dall'Osto, M.; Querol, X.; Alastuey, A.; Perez, N.; Petaja, T.; Massling, A.; Nojgaard, J.K.; et al. The effect of meteorological conditions and atmospheric composition in the occurrence and development of new particle formation (NPF) events in Europe. *Atmos. Chem. Phys.* **2021**, *21*, 3345–3370. [[CrossRef](#)]
33. Zhao, Z.X.; Le, C.; Xu, Q.; Peng, W.H.; Jiang, H.H.; Lin, Y.H.; Cocker, D.R.; Zhang, H.F. Compositional Evolution of Secondary Organic Aerosol as Temperature and Relative Humidity Cycle in Atmospherically Relevant Ranges. *ACS Earth Space Chem.* **2019**, *3*, 2549–2558. [[CrossRef](#)]
34. Liang, L.L.; Engling, G.; Cheng, Y.; Zhang, X.Y.; Sun, J.Y.; Xu, W.Y.; Liu, C.; Zhang, G.; Xu, H.; Liu, X.Y.; et al. Influence of High Relative Humidity on Secondary Organic Carbon: Observations at a Background Site in East China. *J. Meteorol. Res.* **2019**, *33*, 905–913. [[CrossRef](#)]
35. Li, X.X.; Chee, S.; Hao, J.M.; Abbatt, J.P.D.; Jiang, J.K.; Smith, J.N. Relative humidity effect on the formation of highly oxidized molecules and new particles during monoterpene oxidation. *Atmos. Chem. Phys.* **2019**, *19*, 1555–1570. [[CrossRef](#)]
36. Zhang, G.Q.; Fu, H.B.; Chen, J.M. Effect of relative humidity and the presence of aerosol particles on the alpha-pinene ozonolysis. *J. Environ. Sci.* **2018**, *71*, 99–107. [[CrossRef](#)] [[PubMed](#)]
37. Hinks, M.L.; Montoya-Aguilera, J.; Ellison, L.; Lin, P.; Laskin, A.; Laskin, J.; Shiraiwa, M.; Dabdub, D.; Nizkorodov, S.A. Effect of relative humidity on the composition of secondary organic aerosol from the oxidation of toluene. *Atmos. Chem. Phys.* **2018**, *18*, 1643–1652. [[CrossRef](#)]
38. Lewandowski, M.; Jaoui, M.; Offenberg, J.H.; Krug, J.D.; Kleindienst, T.E. Atmospheric oxidation of isoprene and 1,3-butadiene: Influence of aerosol acidity and relative humidity on secondary organic aerosol. *Atmos. Chem. Phys.* **2015**, *15*, 3773–3783. [[CrossRef](#)]
39. Kristensen, K.; Cui, T.; Zhang, H.; Gold, A.; Glasius, M.; Surratt, J.D. Dimers in alpha-pinene secondary organic aerosol: Effect of hydroxyl radical, ozone, relative humidity and aerosol acidity. *Atmos. Chem. Phys.* **2014**, *14*, 4201–4218. [[CrossRef](#)]
40. Li, J.J.; Wang, G.H.; Cao, J.J.; Wang, X.M.; Zhang, R.J. Observation of biogenic secondary organic aerosols in the atmosphere of a mountain site in central China: Temperature and relative humidity effects. *Atmos. Chem. Phys.* **2013**, *13*, 11535–11549. [[CrossRef](#)]
41. Emanuelsson, E.U.; Watne, A.K.; Lutz, A.; Ljungstrom, E.; Hallquist, M. Influence of Humidity, Temperature, and Radicals on the Formation and Thermal Properties of Secondary Organic Aerosol (SOA) from Ozonolysis of beta-Pinene. *J. Phys. Chem. A* **2013**, *117*, 10346–10358. [[CrossRef](#)]
42. Hamed, A.; Korhonen, H.; Sihto, S.L.; Joutsensaari, J.; Jarvinen, H.; Petaja, T.; Arnold, F.; Nieminen, T.; Kulmala, M.; Smith, J.N.; et al. The role of relative humidity in continental new particle formation. *J. Geophys. Res. Atmos.* **2011**, *116*, D03202. [[CrossRef](#)]
43. von Hessberg, C.; von Hessberg, P.; Poschl, U.; Bilde, M.; Nielsen, O.J.; Moortgat, G.K. Temperature and humidity dependence of secondary organic aerosol yield from the ozonolysis of beta-pinene. *Atmos. Chem. Phys.* **2009**, *9*, 3583–3599. [[CrossRef](#)]
44. Pommer, L.; Fick, J.; Andersson, B.; Nilsson, C. The influence of O₃, relative humidity, NO and NO₂ on the oxidation of alpha-pinene and Delta(3)-carene. *J. Atmos. Chem.* **2004**, *48*, 173–189. [[CrossRef](#)]
45. Boy, M.; Kulmala, M. Nucleation events in the continental boundary layer: Influence of physical and meteorological parameters. *Atmos. Chem. Phys.* **2002**, *2*, 1–16. [[CrossRef](#)]
46. Flueckiger, A.C.; Snyder, C.N.; Petrucci, G.A. Nontrivial Impact of Relative Humidity on Organic New Particle Formation from Ozonolysis of cis-3-Hexenyl Acetate. *Air* **2023**, *1*, 222–236. [[CrossRef](#)]
47. Flueckiger, A.; Petrucci, G.A. Methodological advances to improve repeatability of SOA generation in environmental chambers. *Aerosol Sci. Technol.* **2023**, *57*, 925–933. [[CrossRef](#)]
48. Chu, C.W.; Zhai, J.H.; Han, Y.M.; Ye, J.H.; Zaveri, R.A.; Martin, S.T.; Hung, H.M. New Particle Formation and Growth Dynamics for alpha-Pinene Ozonolysis in a Smog Chamber and Implications for Ambient Environments. *ACS Earth Space Chem.* **2022**, *6*, 2826–2835. [[CrossRef](#)]
49. Tillmann, R.; Hallquist, M.; Jonsson, Å.M.; Kiendler-Scharr, A.; Saathoff, H.; Iinuma, Y.; Mentel, T.F. Influence of relative humidity and temperature on the production of pinonaldehyde and OH radicals from the ozonolysis of α -pinene. *Atmos. Chem. Phys.* **2010**, *10*, 7057–7072. [[CrossRef](#)]
50. Tajuelo, M.; Rodriguez, D.; Rodriguez, A.; Escalona, A.; Viteri, G.; Aranda, A.; Diaz-de-Mera, Y. Secondary organic aerosol formation from the ozonolysis and oh-photooxidation of 2,5-dimethylfuran. *Atmos. Environ.* **2021**, *245*, 118041. [[CrossRef](#)]
51. Bianchi, F.; Junninen, H.; Bigi, A.; Sinclair, V.A.; Dada, L.; Hoyle, C.R.; Zha, Q.; Yao, L.; Ahonen, L.R.; Bonasoni, P.; et al. Biogenic particles formed in the Himalaya as an important source of free tropospheric aerosols. *Nat. Geosci.* **2021**, *14*, 4–9. [[CrossRef](#)]

52. Sulo, J.; Sarnela, N.; Kontkanen, J.; Ahonen, L.; Paasonen, P.; Laurila, T.; Jokinen, T.; Kangasluoma, J.; Junninen, H.; Sipila, M.; et al. Long-term measurement of sub-3 nm particles and their precursor gases in the boreal forest. *Atmos. Chem. Phys.* **2021**, *21*, 695–715. [[CrossRef](#)]
53. Artaxo, P.; Hansson, H.C.; Andreae, M.O.; Back, J.; Alves, E.G.; Barbosa, H.M.J.; Bender, F.; Bourtsoukidis, E.; Carbone, S.; Chi, J.S.; et al. Tropical and Boreal Forest Atmosphere Interactions: A Review. *Tellus Ser. B-Chem. Phys. Meteorol.* **2022**, *74*, 24–163. [[CrossRef](#)]
54. Junninen, H.; Ahonen, L.; Bianchi, F.; Quéléver, L.; Schallhart, S.; Dada, L.; Manninen, H.E.; Leino, K.; Lampilahti, J.; Mazon, S.B.; et al. Terpene emissions from boreal wetlands can initiate stronger atmospheric new particle formation than boreal forests. *Commun. Earth Environ.* **2022**, *3*, 00406–00409. [[CrossRef](#)]
55. Kammer, J.; Flaud, P.M.; Chazeaubeny, A.; Ciuraru, R.; Le Menach, K.; Geneste, E.; Budzinski, H.; Bonnefond, J.M.; Lamaud, E.; Perraudin, E.; et al. Biogenic volatile organic compounds (BVOCs) reactivity related to new particle formation (NPF) over the Landes forest. *Atmos. Res.* **2020**, *237*, 104869. [[CrossRef](#)]
56. Liu, Y.F.; Su, H.; Wang, S.W.; Wei, C.; Tao, W.; Pöhlker, M.L.; Pöhlker, C.; Holanda, B.A.; Krüger, O.O.; Hoffmann, T.; et al. Strong particle production and condensational growth in the uppertroposphere sustained by biogenic VOCs from the canopy of the Amazon Basin. *Atmos. Chem. Phys.* **2023**, *23*, 251–272. [[CrossRef](#)]
57. Riipinen, I.; Pierce, J.R.; Yli-Juuti, T.; Nieminen, T.; Häkkinen, S.; Ehn, M.; Junninen, H.; Lehtipalo, K.; Petäjä, T.; Slowik, J.; et al. Organic condensation: A vital link connecting aerosol formation to cloud condensation nuclei (CCN) concentrations. *Atmos. Chem. Phys.* **2011**, *11*, 3865–3878. [[CrossRef](#)]
58. Trostl, J.; Chuang, W.K.; Gordon, H.; Heinritzi, M.; Yan, C.; Molteni, U.; Ahlm, L.; Frege, C.; Bianchi, F.; Wagner, R.; et al. The role of low-volatility organic compounds in initial particle growth in the atmosphere. *Nature* **2016**, *533*, 527–531. [[CrossRef](#)]
59. Dada, L.; Stolzenburg, D.; Simon, M.; Fischer, L.; Heinritzi, M.; Wang, M.; Xiao, M.; Vogel, A.L.; Ahonen, L.; Amorim, A.; et al. Role of sesquiterpenes in biogenic new particle formation. *Sci. Adv.* **2023**, *9*, eadi5297. [[CrossRef](#)] [[PubMed](#)]
60. Quelever, L.L.J.; Kristensen, K.; Jensen, L.N.; Rosati, B.; Teiwes, R.; Daellenbach, K.R.; Perakyla, O.; Roldin, P.; Bossi, R.; Pedersen, H.B.; et al. Effect of temperature on the formation of highly oxygenated organic molecules (HOMs) from alpha-pinene ozonolysis. *Atmos. Chem. Phys.* **2019**, *19*, 7609–7625. [[CrossRef](#)]
61. Yu, S.S.; Jia, L.; Xu, Y.F.; Zhang, H.L.; Zhang, Q.; Pan, Y.P. Wall losses of oxygenated volatile organic compounds from oxidation of toluene: Effects of chamber volume and relative humidity. *J. Environ. Sci.* **2022**, *114*, 475–484. [[CrossRef](#)]
62. Cai, R.L.; Häkkinen, E.; Yan, C.; Jiang, J.K.; Kulmala, M.; Kangasluoma, J. The effectiveness of the coagulation sink of 3–10 nm atmospheric particles. *Atmos. Chem. Phys.* **2022**, *22*, 11529–11541. [[CrossRef](#)]
63. Hennigan, C.J.; Bergin, M.H.; Dibb, J.E.; Weber, R.J. Enhanced secondary organic aerosol formation due to water uptake by fine particles. *Geophys. Res. Lett.* **2008**, *35*, L18801. [[CrossRef](#)]
64. Prisle, N.L.; Engelhart, G.J.; Bilde, M.; Donahue, N.M. Humidity influence on gas-particle phase partitioning of alpha-pinene + O-3 secondary organic aerosol. *Geophys. Res. Lett.* **2010**, *37*, L01802. [[CrossRef](#)]
65. Surdu, M.; Lamkaddam, H.; Wang, D.S.; Bell, D.M.; Xiao, M.; Lee, C.P.; Li, D.; Caudillo, L.; Marie, G.; Scholz, W.; et al. Molecular Understanding of the Enhancement in Organic Aerosol Mass at High Relative Humidity. *Environ. Sci. Technol.* **2023**, *57*, 2297–2309. [[CrossRef](#)] [[PubMed](#)]
66. Han, Y.M.; Gong, Z.H.; Ye, J.H.; Liu, P.F.; McKinney, K.A.; Martin, S.T. Quantifying the Role of the Relative Humidity-Dependent Physical State of Organic Particulate Matter in the Uptake of Semivolatile Organic Molecules. *Environ. Sci. Technol.* **2019**, *53*, 13209–13218. [[CrossRef](#)] [[PubMed](#)]
67. Wang, N.X.; Jorga, S.D.; Pierce, J.R.; Donahue, N.M.; Pandis, S.N. Particle wall-loss correction methods in smog chamber experiments. *Atmos. Meas. Tech.* **2018**, *11*, 6577–6588. [[CrossRef](#)]
68. Seinfeld, J.H.; Erdakos, G.B.; Asher, W.E.; Pankow, J.F. Modeling the formation of secondary organic aerosol (SOA). 2. The predicted effects of relative humidity on aerosol formation in the alpha-pinene-, beta-pinene-, sabinene-, Delta(3)-Carene-, and cyclohexene-ozone systems. *Environ. Sci. Technol.* **2001**, *35*, 1806–1817. [[CrossRef](#)] [[PubMed](#)]
69. Jathar, S.H.; Mahmud, A.; Barsanti, K.C.; Asher, W.E.; Pankow, J.F.; Kleeman, M.J. Water uptake by organic aerosol and its influence on gas/particle partitioning of secondary organic aerosol in the United States. *Atmos. Environ.* **2016**, *129*, 142–154. [[CrossRef](#)]
70. Pankow, J.F.; Marks, M.C.; Barsanti, K.C.; Mahmud, A.; Asher, W.E.; Li, J.Y.; Ying, Q.; Jathar, S.H.; Kleeman, M.J. Molecular view modeling of atmospheric organic particulate matter: Incorporating molecular structure and co-condensation of water. *Atmos. Environ.* **2015**, *122*, 400–408. [[CrossRef](#)]
71. Qin, Y.; Ye, J.; Ohno, P.; Zhai, J.; Han, Y.; Liu, P.; Wang, J.; Zaveri, R.A.; Martin, S.T. Humidity Dependence of the Condensational Growth of α -Pinene Secondary Organic Aerosol Particles. *Environ. Sci. Technol.* **2021**, *55*, 14360–14369. [[CrossRef](#)]
72. Pankow, J.F. Organic particulate material levels in the atmosphere: Conditions favoring sensitivity to varying relative humidity and temperature. *Proc. Natl. Acad. Sci. USA* **2010**, *107*, 6682–6686. [[CrossRef](#)] [[PubMed](#)]
73. Gong, Z.H.; Han, Y.M.; Liu, P.F.; Ye, J.H.; Keutsch, F.N.; McKinney, K.A.; Martin, S.T. Influence of Particle Physical State on the Uptake of Medium-Sized Organic Molecules. *Environ. Sci. Technol.* **2018**, *52*, 8381–8389. [[CrossRef](#)] [[PubMed](#)]
74. Zaveri, R.A.; Shilling, J.E.; Zelenyuk, A.; Liu, J.M.; Bell, D.M.; D'Ambro, E.L.; Gaston, C.; Thornton, J.A.; Laskin, A.; Lin, P.; et al. Growth Kinetics and Size Distribution Dynamics of Viscous Secondary Organic Aerosol. *Environ. Sci. Technol.* **2018**, *52*, 1191–1199. [[CrossRef](#)] [[PubMed](#)]

75. Zaveri, R.A.; Shilling, J.E.; Zelenyuk, A.; Zawadowicz, M.A.; Suski, K.; China, S.; Bell, D.M.; Veghte, D.; Laskin, A. Particle-Phase Diffusion Modulates Partitioning of Semivolatile Organic Compounds to Aged Secondary Organic Aerosol. *Environ. Sci. Technol.* **2020**, *54*, 2595–2605. [[CrossRef](#)] [[PubMed](#)]
76. Kerminen, V.M.; Lehtinen, K.E.J.; Anttila, T.; Kulmala, M. Dynamics of atmospheric nucleation mode particles: A timescale analysis. *Tellus B Chem. Phys. Meteorol.* **2004**, *56*, 135–146. [[CrossRef](#)]
77. Kürten, A.; Williamson, C.; Almeida, J.; Kirkby, J.; Curtius, J. On the derivation of particle nucleation rates from experimental formation rates. *Atmos. Chem. Phys.* **2015**, *15*, 4063–4075. [[CrossRef](#)]
78. Charan, S.M.; Huang, Y.L.; Seinfeld, J.H. Computational Simulation of Secondary Organic Aerosol Formation in Laboratory Chambers. *Chem. Rev.* **2019**, *119*, 11912–11944. [[CrossRef](#)]

Disclaimer/Publisher’s Note: The statements, opinions and data contained in all publications are solely those of the individual author(s) and contributor(s) and not of MDPI and/or the editor(s). MDPI and/or the editor(s) disclaim responsibility for any injury to people or property resulting from any ideas, methods, instructions or products referred to in the content.